Numerical experiments on subaqueous melting of Greenland tidewater glaciers in response to ocean warming and enhanced subglacial discharge

Yun XU,[1] Eric RIGNOT,[1,2] Dimitris MENEMENLIS,[2] Michele KOPPES[3]

[1] *Earth System Science, University of California, Irvine, Irvine, CA, USA*
E-mail: yunx@uci.edu
[2] *Jet Propulsion Laboratory, California Institute of Technology, Pasadena, CA, USA*
[3] *Department of Geography, University of British Columbia, Vancouver, British Columbia, Canada*

ABSTRACT. The largest dischargers of ice in Greenland are glaciers that terminate in the ocean and melt in contact with sea water. Studies of ice-sheet/ocean interactions have mostly focused on melting beneath near-horizontal floating ice shelves. For tidewater glaciers, melting instead takes place along the vertical face of the calving front. Here we modify the Massachusetts Institute of Technology general circulation model (MITgcm) to include ice melting from a calving face with the freshwater outflow at the glacier grounding line. We use the model to predict melt rates and their sensitivity to ocean thermal forcing and to subglacial discharge. We find that melt rates increase with approximately the one-third power of the subglacial water flux, and increase linearly with ocean thermal forcing. Our simulations indicate that, consistent with limited field data, melting ceases when subglacial discharge is shut off, and reaches several meters per day when subglacial discharge is high in the summer. These results are a first step toward a more realistic representation of subglacial discharge and of ocean thermal forcing on the subaqueous melting of tidewater glaciers in a numerical ocean model. Our results illustrate that the ice-front melting process is both complex and strongly time-dependent.

INTRODUCTION

The mass loss from the Greenland ice sheet has increased rapidly in the last two decades (Velicogna, 2009), largely due to the widespread acceleration of Greenland's tidewater (i.e. marine-terminating) glaciers (Rignot and Kanagaratnam, 2006) and due to an increase in surface meltwater runoff (Van den Broeke and others, 2009). Holland and others (2008a) hypothesized that ocean warming caused the collapse of the floating ice tongue in front of Jakobshavn Isbræ and triggered an acceleration of Greenland's largest tidewater glacier. Yet, little is known about rates of subaqueous melting of these marine-terminating glaciers, and there are virtually no quantitative estimates of the mechanical impact of subaqueous melting on glacier dynamics. Vigorous subaqueous melting may control glacier retreat rates and the position of the grounding line, which, in turn, would control flow speeds near the terminus (Nick and others, 2009).

In Alaska, Motyka and others (2003) analyzed oceanographic data in front of LeConte Glacier to estimate a subaqueous melt rate of $12\,\mathrm{m\,d^{-1}}$ across the calving face during the summer of 2000, which represented half of the total ice mass flux through the glacier terminus. In Greenland, Rignot and others (2010) estimated rates of subaqueous melting from three major tidewater glaciers in a similar manner, and found melt values ranging from 0.7 to $3.5\,\mathrm{m\,d^{-1}}$ on the calving faces during the summer of 2008, which corresponded to 20–80% of the total ice volume flux to the glacier termini. These results illustrate the significance of subaqueous melting for tidewater glaciers (i.e. a significant component of mass loss) and highlight the need for more quantitative studies of ice melting and its sensitivity to both ocean and climate forcings, so that this knowledge can be included in numerical models of ice-sheet evolution.

In this study we modify an existing ocean general circulation model, the Massachusetts Institute of Technology general circulation model (MITgcm), to include the processes of subaqueous melting, by which we are referring to melting along the vertical calving face of tidewater glaciers. We apply the MITgcm to a realistic simplification of a glacial fjord in West Greenland to predict melt rates along the calving face of the glacier at the head of the fjord and how these melt rates vary with ocean thermal forcing and with subglacial freshwater discharge.

MODEL AND METHODS

Ice-front melt parameterization

The MITgcm (Marshall and others, 1997b,a) includes a representation of freezing and melting at the near-horizontal base of floating ice shelves (Losch, 2008). The three-equation formulation, which is used to represent freezing and melting below floating ice shelves (e.g. Holland and others, 2008b), can also be applied to represent freezing and melting of a vertical face, because the boundary layer structures are similar (Wells, 2008). For this study we add a new module to the MITgcm that represents the vertical ice/ocean boundary using:

$$T_\mathrm{B} = aS_\mathrm{B} + b + cp_\mathrm{B} \quad (1)$$

$$C_{p\mathrm{W}}\rho\gamma_\mathrm{T}|w|(T - T_\mathrm{B}) = -q\left[L_\mathrm{f} + C_{p\mathrm{I}}(T_\mathrm{ice} - T_\mathrm{B})\right] \quad (2)$$

$$\rho\gamma_\mathrm{S}|w|(S - S_\mathrm{B}) = -q(S_\mathrm{B} - S_\mathrm{ice}) \quad (3)$$

Equation (1) states that temperature at the ice/ocean boundary is at the local melting/freezing point, which is a linear function of salinity and pressure. Equation (2) is the conservation of heat, which states that the heat flux at the ice/ocean boundary brings ice or water to the melting point and melts or

https://doi.org/10.3189/2012AoG60A139 Published online by Cambridge University Press

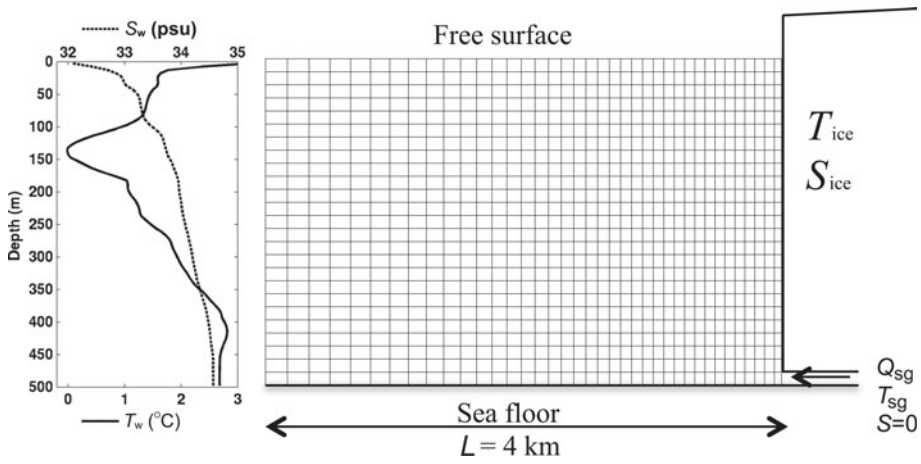

Fig. 1. Model domain for the MITgcm with the temperature (T_W) and salinity (S_W) forcing at the open ocean boundary (left-hand side, fjord entrance); model mesh (actual mesh is 4× denser) in the fjord; sea surface, sea floor and ice/ocean boundary (right-hand side).

freezes it. Equation (3) is the conservation of salinity, which states that the boundary layer salinity balances the salinity of freezing or melting ice and the salinity of ambient sea water. The heat and salinity transfer coefficients, γ_T and γ_S respectively, follow the values of $C_d^{1/2}\Gamma_T$ and $C_d^{1/2}\Gamma_S$ in the work of Jenkins and others (2010). Definitions of the variables used, units and parameter values are given in Table 1. Equations (1–3) are solved at the vertical ice/ocean boundary in order to obtain estimates of freezing or melting rate.

Model configuration

The MITgcm modified with subaqueous melting on vertical ice walls is applied to a simplified glacial fjord geometry. The goals are to produce model estimates of the melt rate and to test the sensitivity of the model results to ocean thermal forcing and subglacial discharge. We base our model geometry on the general configuration of the glacial fjord in front of Store Glacier (70°22′ N, 50°38′ W), West Greenland, which we surveyed by boat in August 2010. The glacier is ∼5 km wide at the ice front. The fjord extends 60 km westward to the open ocean and is 400–600 m deep near the ice front. The location and depth of any sills in the outer fjord are unknown at this time. In our numerical experiments, the fjord is 500 m deep and 6.4 km long. Model grid spacing is 5 m in the vertical and 20 m in the horizontal along the fjord near the calving front, gradually increasing to 50 m at the open ocean boundary of our domain, illustrated in Figure 1. The model configuration is two-dimensional, i.e. there is no variability in the across-fjord direction, and no Coriolis force.

We collected temperature and salinity profiles with a Seabird SBE-19 conductivity, temperature and depth (pressure) profiler 4 km from the Store Glacier front on 18 August 2010 (Fig. 1). These measurements are used as initial conditions, as well as boundary conditions, for our model. Ice temperature at the calving front is set at −2°C the temperature typically measured in outlet glaciers in coastal Greenland (Thomsen and Thorning, 1992).

The model is integrated as a free surface and non-hydrostatic configuration. Dynamic viscosity is chosen to approach minimum values to avoid gridscale noise when modeling the fastest subglacial discharge. We choose a vertical viscosity of 0.1 $m^2\,s^{-1}$, and a horizontal biharmonic viscosity of 300 $m^4\,s^{-1}$. Diffusivity is set to equal the viscosity to make the Prandtl number equal to one for the turbulent plume.

Table 1. Parameters and variables used in Eqns (1–3)

Symbol	Description	Value	Unit
L_f	Latent heat of water	334 000	J kg^{-1}
C_{pI}	Heat capacity of ice	2000	J kg^{-1} °C^{-1}
C_{pW}	Heat capacity of water	3994	J kg^{-1} °C^{-1}
a	Parameter for freezing point	−0.0575	°C psu^{-1}
b	Parameter for freezing point	0.0901	°C
c	Parameter for freezing point	-7.61×10^{-4}	°C dbar^{-1}
γ_T	Heat transfer coefficient	1.1×10^{-3}	
γ_S	Salinity transfer coefficient	3.1×10^{-5}	
w	Vertical velocity along the ice face		m s^{-1}
ρ	Sea-water density		kg m^{-3}
p_B	Local pressure		dbar
T_B	Boundary layer temperature		°C
T	Sea-water temperature		°C
T_{ice}	Ice temperature		°C
S	Sea-water salinity		psu
S_B	Boundary layer salinity		psu
S_{ice}	Ice salinity	0	psu
q	Melting rate of ice		kg m^{-2} s^{-1}

Subglacial discharge

We implement subglacial discharge as a flux of fresh water at the pressure-dependent melting-point temperature and inject this discharge horizontally into the ocean at the base of the vertical ice face. Specifically, the subglacial flux is fixed by the size of the subglacial channel (i.e. tunnel), where fresh water is injected at the glacier base, and the velocity of that subglacial water flow.

We use estimates of surface runoff from the Regional Atmospheric Climate Model (RACMO) (Ettema and others, 2009) as a proxy for the subglacial water flux, Q_{sg}. We assume that (1) all glacier surface meltwater collects at the glacier bed upstream of the glacier terminus and (2) subglacial meltwater channels merge into a few large channels before reaching the terminus, as is commonly observed at land-terminating glaciers. At Store Glacier, Q_{sg} may reach 500 $m^3\,s^{-1}$ in summer and drops to ∼0 $m^3\,s^{-1}$ in winter; the average discharge during the May–September melting season is 200 $m^3\,s^{-1}$. The large seasonal variability of Q_{sg} is consistent with observations conducted on nearby

https://doi.org/10.3189/2012AoG60A139 Published online by Cambridge University Press

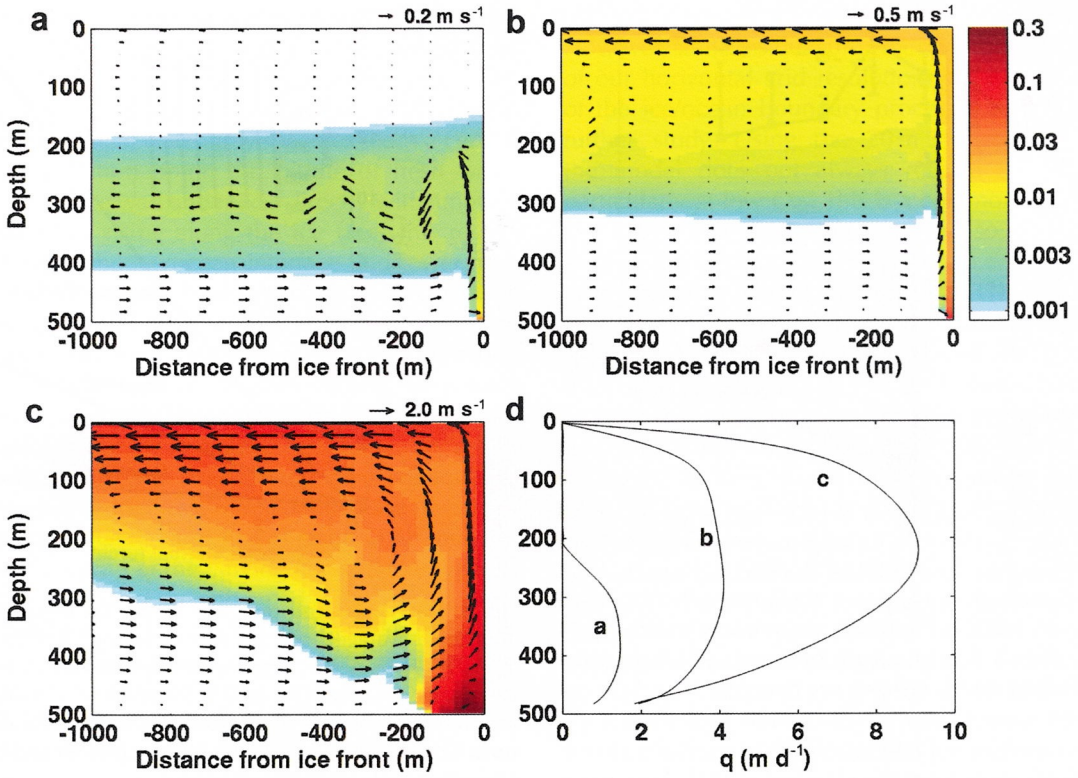

Fig. 2. Modeled ocean circulation in front of the glacier for a subglacial flux, Q_{sg}, of (a) 0.5 m s^{-1}, (b) 5 m s^{-1} and (c) 150 m s^{-1}, overlaid on the mixing ratio in volume of subglacial water vs sea water, color-coded from white (zero) to brown (0.3). (d) The water-equivalent melt rate, q (m d^{-1}), vs depth along the ice/ocean interface for cases (a), (b) and (c). Arrows represent the water velocity.

land-terminating glaciers (Mernild and Hasholt, 2009). From our boat survey in August 2010, we identified at least two main channels of subglacial outflow along the north and south edges of the terminus of Store Glacier; there could be more. We therefore expect the freshwater flux from each channel to average 100 m^3 s^{-1} from May to September, with peak values approaching 250 m^3 s^{-1} in midsummer.

Röthlisberger (1972) established a theoretical framework to estimate the size of subglacial channels in steady state by assuming that the rate of closure of the channel caused by ice deformation is balanced by the rate of opening from melting of the inner face. Here we use an ice/water pressure difference of 50 dbar, ice deformation rate of 727 bar s$^{1/3}$, and channel roughness of 0.02 (Röthlisberger, 1972, and references therein) to calculate a typical channel size, which we find to be ~50 m^2 in steady state for our average Q_{sg} of 100 m^3 s^{-1}, and 100 m^2 for our maximum Q_{sg} of 250 m^3 s^{-1}. As direct underwater observations of subglacial channel size or flow speeds are difficult to conduct and have not been done at any calving glacier termini to date, we bound the range of possible channel sizes from observations of circular or semicircular subglacial channels at the outlets of land-terminating glaciers, which are typically several meters in diameter (e.g. Näslund and Hassinen, 1996). The sizes of these channels change over timescales of several months, while the subglacial water flux, Q_{sg}, typically changes over timescales of hours to days. Therefore, channel size can be assumed to be constant throughout the 5 day period of integration of each model run.

In order to test the influence of uncertainty in channel size on our estimates of the subaqueous melt rate, we tested three rectangular channel sizes in our model: 25 m^2 (2.5 m × 10 m), 50 m^2 (5 m × 10 m) and 100 m^2 (10 m × 10 m). Within each channel, subglacial water is at the pressure-dependent melting point (−0.28°C), with zero salinity. The speed of the flow in the subglacial channel is varied from 0 to 4 m s^{-1}, which changes subglacial water flux, Q_{sg}. The added water flux from the subglacial channel is removed evenly at all depths along the open ocean boundary at the distal end of the fjord to avoid having excess water build up in the fjord.

Sensitivity analyses

In a first set of experiments designed to test the influence of subglacial discharge, we keep the temperature and salinity profile at the ocean boundary constant and only vary the subglacial water flux, Q_{sg}. Each sensitivity experiment is initialized with the temperature and salinity profiles collected in 2010 and shown in Figure 1 (left panel). In a second set of experiments, we keep the subglacial water flux and the ocean salinity constant, and linearly vary the deviation of ocean temperature from the in situ pressure-melting point from 0 to 8°C, as shown in the inset in Figure 4. We run each ocean-warming experiment with a subglacial channel size of 50 m^2 and with three values of subglacial discharge corresponding to 0.5, 5 and 25 m^3 s^{-1}. The ocean-warming experiments are initialized with the temperature profiles shown in the inset of Figure 4. Each sensitivity experiment is integrated for 5 days, until it reaches a quasi-equilibrium indicated by a stable melt rate and ocean circulation.

RESULTS

When subglacial discharge is near zero, the model generates little convection in front of the glacier and the melt rate is very low. As soon as a small amount of subglacial discharge is added (Fig. 2a), fresh water rises along the ice/ocean interface

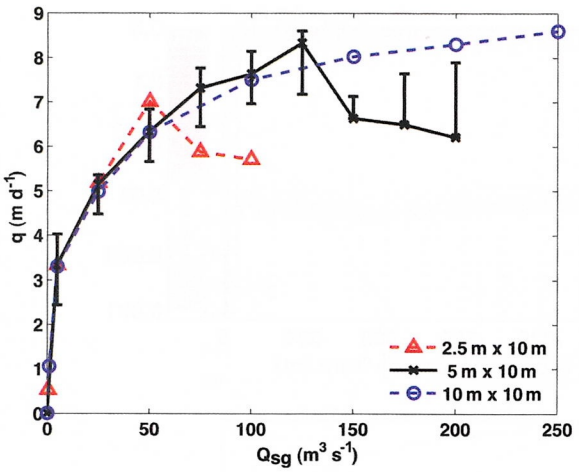

Fig. 3. Depth-averaged melt rate of the ice front, q (m w.e. d^{-1}), and subglacial flux, Q_{sg} ($m^3\ s^{-1}$), for subglacial channels of various sizes. Error bars using the 50 m^2 channel size scenario were derived by varying the horizontal viscosity from 100 to 900 $m^4\ s^{-1}$ (except for when $Q_{sg} > 150\ m^3\ s^{-1}$, where the minimum viscosity is limited to 300 $m^4\ s^{-1}$). At high subglacial fluxes, when subglacial flow speeds exceed 2 m s^{-1}, the melt rate decreases.

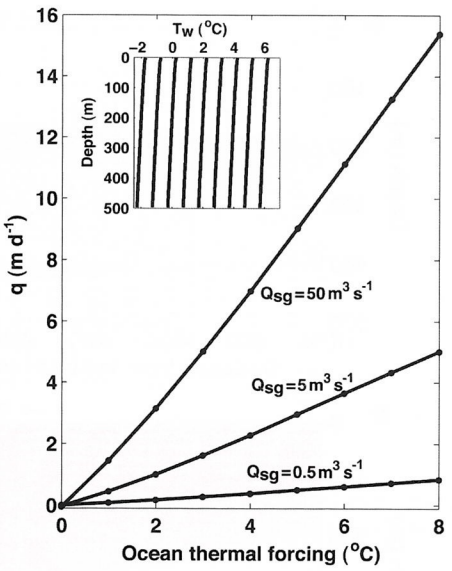

Fig. 4. Depth-averaged melt rate of the ice front, q (m w.e. d^{-1}), and depth-averaged ocean thermal forcing, T_F (°C), where $T_F = T_w - T_f$ (T_w is ocean temperature, T_f is sea-water freezing point), for subglacial fluxes, Q_{sg}, of 0.5, 5 and 50 $m^3\ s^{-1}$. Inset plot shows the change in ocean temperature, T_w, vs depth for different model runs. $T_F = 0$ in the initial run (leftmost profile) and is increased in 1°C increments for each subsequent run.

and drives bottom ocean water to flow toward the ice face. Fresh water from melted ice and subglacial discharge mixes with the ambient sea water before flowing away from the ice face at some intermediate depth in a stratified ocean. Subaqueous ice melting takes place at depths below 200 m, where upwelling is present at the ice front (Fig. 2d). As Q_{sg} increases, upwelling along the ice/ocean interface increases in speed and reaches shallower depths below the ocean surface. This upwelling drives stronger ocean circulation, manifested by a larger volume of sea water entrained toward the ice and by higher flow speeds. When Q_{sg} approaches ~5 $m^3\ s^{-1}$ (Fig. 2b), upwelling forces fresh water all the way to the ocean surface and this water subsequently flows away from the ice along the ocean surface. The calculated melt rate averages ~4 m d^{-1} at all depths, except near the top and the bottom of the ice face (Fig. 2d). When Q_{sg} increases to 150 $m^3\ s^{-1}$, which corresponds to a flow speed in the subglacial channel of 3 m s^{-1}, the freshwater plume moves horizontally off the ice face near the ocean bottom for ~100 m, mixes with ambient sea water, and forms a broad, rising plume (Fig. 2c). The maximum melt rate in this instance occurs at mid-depths and approaches 9 m d^{-1} (Fig. 2d).

When we compile the results obtained by varying Q_{sg} from 0 to 250 $m^3\ s^{-1}$ (Fig. 3), we find that the depth-averaged melt rate increases with Q_{sg} in a nonlinear fashion. A reasonable fit is obtained with a power law of ~1/3 for low subglacial fluxes, consistent with Jenkins (2011), who used a simplified one-dimensional convection-driven plume model and found the cube-root dependence of subaqueous melt rate on the subglacial discharge. Increasing or decreasing the horizontal viscosity by a factor of three changes the calculated melt rates by <10%, as indicated by the error bars on the results, using a channel size of 50 m^2, in Figure 3.

In Figure 3, we also compare the results using the three different sizes of subglacial channels. For low values of Q_{sg}, all three curves have a similar shape, which suggests that the melt rate is not sensitive to channel size or flow speed when the subglacial flux is low. As Q_{sg} increases to 50 $m^3\ s^{-1}$, the results using the smallest channel size (25 m^2) start to diverge. With a smaller channel size, and therefore a higher subglacial flow speed at a constant flux, subglacial water tends to move horizontally away from the ice face near the ocean bottom when $Q_{sg} > 50\ m^3\ s^{-1}$, and melting becomes less efficient. With a larger channel size, this saturation point for the melt rate occurs at higher values of subglacial flux (e.g. melting becomes less efficient when Q_{sg} exceeds 125 $m^3\ s^{-1}$ for a 50 m^2 channel). In our second set of ocean-warming experiments, we linearly increase the ocean temperature from the in situ freezing point of sea water to 8°C above the freezing point (Fig. 4). This is a direct measure of ocean thermal forcing, which we define as the difference between the ambient ocean temperature, T_w, and the pressure-dependent melting point of sea water, T_f. The results, shown in Figure 4, indicate that no subaqueous melting occurs when the thermal forcing is zero, and melting increases linearly as ocean thermal forcing increases.

DISCUSSION

Our model experiments indicate that subglacial discharge plays an important role in ocean circulation near the glacier calving front, and in determining the rate of subaqueous melting of the glacier calving face. In winter, when subglacial discharge is negligible, the model predicts very low melt rates. This is consistent the observations of Walters and others (1988) during winter at Columbia Glacier, Alaska. We are not aware of any other studies at glacier termini that measured ice-front melting in winter. During late spring, summer and early fall, when subglacial discharge is significant, our model suggests that subaqueous melting rapidly becomes a substantial component of overall ice mass loss. The melt rates observed (Rignot and others, 2010) and simulated (this paper) range from one to several meters per day for Greenland's tidewater glaciers.

https://doi.org/10.3189/2012AoG60A139 Published online by Cambridge University Press

We find a sub-linear dependence of the melt rate on the subglacial flux, where the melt rate does not increase as rapidly as the subglacial discharge. In our simulations with a fixed channel size, we also find a 'saturation' point for melt rates when the subglacial water flow speed exceeds a certain value. At this saturation point, the plume of fresh water 'detaches' from the ice wall and mixes directly with ambient sea water instead of rising along the ice face; this results in less upwelling at the ice/ocean interface and lower melt rates. Given that we do not have any direct measurements of the size of subglacial outflow channels or the speed of subglacial water flow from any tidewater glacier, let alone any seasonal measurements of ice-front melting, we cannot confirm whether such a saturation point is ever reached during the summer months in reality.

An interesting corollary to the dependence of subaqueous melting on subglacial discharge is that an increase in surface runoff production in Greenland would result in an increase in ocean-forced melting of the calving faces of the glaciers. It is therefore possible that the enhanced runoff experienced by the Greenland ice sheet in the last two decades may have indirectly impacted the stability of ice fronts in Greenland by enhancing subaqueous melt rates.

As revealed in our model, most of the buoyant freshwater plumes rise right along the ice face. Several lines of evidence provide support for this model result. One is a common observation of a significant rise in sea surface height (as high as 1 m) at the calving fronts of marine-terminating glaciers (personal communication from R. Motyka, 2011). This is a robust and repeating feature in our model results. A second line of evidence is the presence of pronounced fluting on the vertical ice face, which is observed in overturned icebergs (personal communication from R. Motyka, 2011). This fluting pattern is consistent with a spatial pattern of buoyant fresh water rising along the submerged ice face and melting the ice along vertically oriented preferential paths incised into the ice face.

Straneo and others (2011) observe two distinct layers of fresh water near the surface and at 200 m depth near the front of Helheim Glacier, East Greenland. This is also a feature that can be explained by our model results, where not all the fresh water resulting from melting of the ice face reaches the ocean surface. Instead, a portion of the meltwater approaches an equilibrium in density with ambient sea water at some intermediate depth in the fjord. Depending on the flow speed, the outflow of subglacial fresh water from the glacier can emerge along the ice front, mix with ambient water at some intermediate depth, and/or reach the surface at a distance from the ice front. In reality, the distribution of subglacial discharge is likely more complex than assumed in our model, and we would expect to find a mixed regime of fresh water and sea water stabilizing at a variety of depths in the fjord.

We also find that the melt rate increases linearly with ocean warming, a conclusion also reached by Jenkins (2011) using a convection-driven plume model. We believe this linear dependence of melt on ocean forcing is robust, because the flow speed of fresh water along the ice face does not increase in proportion to the ocean thermal forcing; if it did, we would expect the relationship between thermal forcing and melt rates to be quadratic.

These results are robust, no matter which values of horizontal viscosity and diffusivity are applied in the model; the melt rates changed by $<10\%$ when the viscosity and diffusivity parameters were varied by a factor of three. However, some residual uncertainties related to the selection of our horizontal grid resolution and the parameterization of the ice/ocean boundary processes remain, that require further study. Using the 20 m horizontal grid spacing, the model does not always resolve convective plumes, particularly at low Q_{sg}. This is a common attribute of ocean circulation models. To test this, we also ran the model with a $10\times$ finer horizontal resolution, i.e. at 2 m horizontal resolution. In so doing, we found that (1) the general pattern of ocean circulation remained unchanged, i.e. the grid spacing does not affect the speed when the plume detaches from the ice wall; (2) at 2 m grid spacing, we were able to resolve the plume (i.e. it is seen spreading over several gridcells) at high Q_{sg} but not at very low Q_{sg}; (3) the melt rate increased by 39–75%, or 60% on average; however (4) the melt rate displayed the same cubic-root dependence on the subglacial flux.

In all our sensitivity experiments, we use the velocity, temperature and salinity results from the first gridcell next to the ice face to calculate the melt rate. The parameterization values we used for the heat and salt transfer coefficients, γ_T and γ_S, in Eqns (1–3) are the same as those calculated by Jenkins and others (2010), which were obtained based on observations under horizontal ice shelves, with a velocity measured at 20 m and a temperature measured at 1.9 m from the bottom of the ice shelf. We employ the same transfer parameters in all our numerical experiments, regardless of the width of the first gridcell adjacent to the vertical ice face, although we expect that decreasing the horizontal grid spacing would produce higher melting rates. In the absence of direct measurements of ice melt to compare with our model, we decided not to adjust these parameters. While this could be a significant source of uncertainty in our model results, we note that our simulations suggest that the choice of heat and salt transfer parameters does not affect the nature of the relationship between melt rates and subglacial discharge, nor between melt rates and ocean thermal forcing, which is the focus of this study.

We note that, for simplicity, several other factors of potential importance have not been considered in this study. One potential contributing factor is ocean tides, since tidal currents may affect the ventilation of the ice cavity (Straneo and others, 2010). Another potential factor is winds, particularly katabatic winds that could affect the motion of the surface waters in front of the glaciers and within the fjords. Similarly, we did not investigate the impact of fjord bathymetry or the presence of sills. Most importantly, our model is two-dimensional, whereas melting at the ice/ocean boundary is expected to be three-dimensional, due to turbulence of the freshwater plumes, the injection of subglacial discharge along the ice face at discrete locations, and the presence of ocean eddies near the ice face. All these aspects will be addressed and evaluated in future studies.

CONCLUSION

In this study, we modified the MITgcm to include ice melting along the vertical face of a marine-terminating glacier forced by the discharge of subglacial fresh water at the glacier base. The model reveals important features about the pattern of ocean circulation in front of the glacier, the rates of subaqueous melting that might be expected, and how this melt rate depends on subglacial discharge and

https://doi.org/10.3189/2012AoG60A139 Published online by Cambridge University Press

ocean temperature. The model indicates (1) high rates of subaqueous melting (meters per day) in the summer months, (2) negligible melting in winter, (3) a cube-root dependence on subglacial discharge and (4) a linear dependence on ocean thermal forcing. These results, combined with the recent study of Jenkins (2011), help provide first-order constraints on how a warmer climate and warmer ocean may affect the melting of calving fronts of tidewater glaciers and, in turn, affect the grounding-line stability and flow speeds of these outlet glaciers, with repercussions for the stability of the Greenland ice sheet as a whole.

ACKNOWLEDGEMENTS

This work was performed at the Department of Earth System Science, University of California, Irvine, and the California Institute of Technology Jet Propulsion Laboratory under a contract with the National Aeronautics and Space Administration Cryosphere Science Program. We thank M. van den Broeke for RACMO data. We also thank T. and C. Jensen for their assistance in data collection in Greenland in 2010.

REFERENCES

Ettema J and 6 others (2009) Higher surface mass balance of the Greenland ice sheet revealed by high-resolution climate modelling. *Geophys. Res. Lett.*, **36**(12), L12501 (doi: 10.1029/2009GL038110)

Holland DM, Thomas RH, de Young B, Ribergaard MH and Lyberth B (2008a) Acceleration of Jakobshavn Isbræ triggered by warm subsurface ocean waters. *Nature Geosci.*, **1**(10), 659–664 (doi: 10.1038/ngeo316)

Holland PR, Jenkins A and Holland DM (2008b) The response of ice shelf basal melting to variations in ocean temperature. *J. Climate*, **21**(11), 2558–2572 (doi: 10.1175/2007JCLI1909.1)

Jenkins A (2011) Convection-driven melting near the grounding lines of ice shelves and tidewater glaciers. *J. Phys. Oceanogr.*, **41**(12), 2279–2294 (doi: 10.1175/JPO-D-11-03.1)

Jenkins A, Nicholls KW and Corr HFJ (2010) Observation and parameterization of ablation at the base of Ronne Ice Shelf, Antarctica. *J. Phys. Oceanogr.*, **40**(10), 2298–2312 (doi: 10.1175/2010JPO4317.1)

Losch M (2008) Modeling ice shelf cavities in a *z* coordinate ocean general circulation model. *J. Geophys. Res.*, **113**(C8), C08043 (doi: 10.1029/2007JC004368)

Marshall J, Adcroft A, Hill C, Perelman L and Heisey C (1997a) A finite-volume, incompressible Navier Stokes model for studies of the ocean on parallel computers. *J. Geophys. Res.*, **102**(C3), 5753–5766

Marshall J, Hill C, Perelman L and Adcroft A (1997b) Hydrostatic, quasi-hydrostatic, and nonhydrostatic ocean modeling. *J. Geophys. Res.*, **102**(C3), 5733–5752 (doi: 10.1029/96JC02776)

Mernild SH and Hasholt B (2009) Observed runoff, jökulhlaups and suspended sediment load from the Greenland ice sheet at Kangerlussuaq, West Greenland, 2007 and 2008. *J. Glaciol.*, **55**(193), 855–858 (doi: 10.3189/002214309790152465)

Motyka RJ, Hunter L, Echelmeyer KA and Connor C (2003) Submarine melting at the terminus of a temperate tidewater glacier, LeConte Glacier, Alaska, USA. *Ann. Glaciol.*, **36**, 57–65 (doi: 10.3189/172756403781816374)

Näslund, JO and Hassinen S (1996) Correspondence. Supraglacial sediment accumulations and large englacial water conduits at high elevations in Mýrdalsjökull, Iceland. *J. Glaciol.*, **42**(140), 190–192

Nick FM, Vieli A, Howat IM and Joughin I (2009) Large-scale changes in Greenland outlet glacier dynamics triggered at the terminus. *Nature Geosci.*, **2**(2), 110–114 (doi: 10.1038/ngeo394)

Rignot E and Kanagaratnam P (2006) Changes in the velocity structure of the Greenland Ice Sheet. *Science*, **311**(5673), 986–990 (doi: 10.1126/science.1121381)

Rignot E, Koppes M and Velicogna I (2010) Rapid submarine melting of the calving faces of West Greenland glaciers. *Nature Geosci.*, **3**(3), 141–218 (doi: 10.1038/ngeo765)

Röthlisberger H (1972) Water pressure in intra- and subglacial channels. *J. Glaciol.*, **11**(62), 177–203

Straneo F and 7 others (2010) Rapid circulation of warm subtropical waters in a major glacial fjord in East Greenland. *Nature Geosci.*, **3**(33), 182–186 (doi: 10.1038/ngeo764)

Straneo F and 6 others (2011) Impact of fjord dynamics and glacial runoff on the circulation near Helheim Glacier. *Nature Geosci.*, **4**(5), 322–327 (doi: 10.1038/ngeo1109)

Thomsen HH and Thorning L (1992) Ice temperature profiles for western Greenland. *Grønl. Geol. Unders. Rapp.*

Van den Broeke M and 8 others (2009) Partitioning recent Greenland mass loss. *Science*, **326**(5955), 984–986 (doi: 10.1126/science.1178176)

Velicogna I (2009) Increasing rates of ice mass loss from the Greenland and Antarctic ice sheets revealed by GRACE. *Geophys. Res. Lett.*, **36**(19), L19503 (doi: 10.1029/2009GL040222)

Walters RA, Josberger EG and Driedger CL (1988) Columbia Bay, Alaska: an 'upside down' estuary. *Estuar. Coast. Shelf Sci.*, **26**(6), 607–617

Wells AJ (2008) Natural convection boundary layers and their influence on phase change in the polar oceans. (PhD thesis, University of Cambridge)